EU FT-ICR MS

AUS2- Prague, 26-30 September 2021

Exploring the intrinsic properties of bioinorganic complexes by Ion-Molecule Reactions

SAPIENZA
UNIVERSITÀ DI ROMA

Maria Elisa Crestoni

Dipartimento di Chimica e Tecnologie del Farmaco,
Sapienza Università di Roma, P.le A. Moro 5, I-00185, Roma (Italy)

Ion-Molecule Reactions

- First observation (Thomson, 1913)
- Chemical Ionization Source (Munson and Field, 1966)
- Multiple-stage Mass Spectrometers (ion isolation + reactions with specific gaseous reagent under low-energy, controlled conditions)
- High degree of experimental flexibility

The Gas Phase, in the absence of solvent and counterions, allows to elucidate the **intrinsic behavior in ionic reactions** and expose the role of the environment.

M.S.B. Munson, F. H. Field, J. Am. Chem. Soc. 1966;
J. I. Brauman, Science 1998

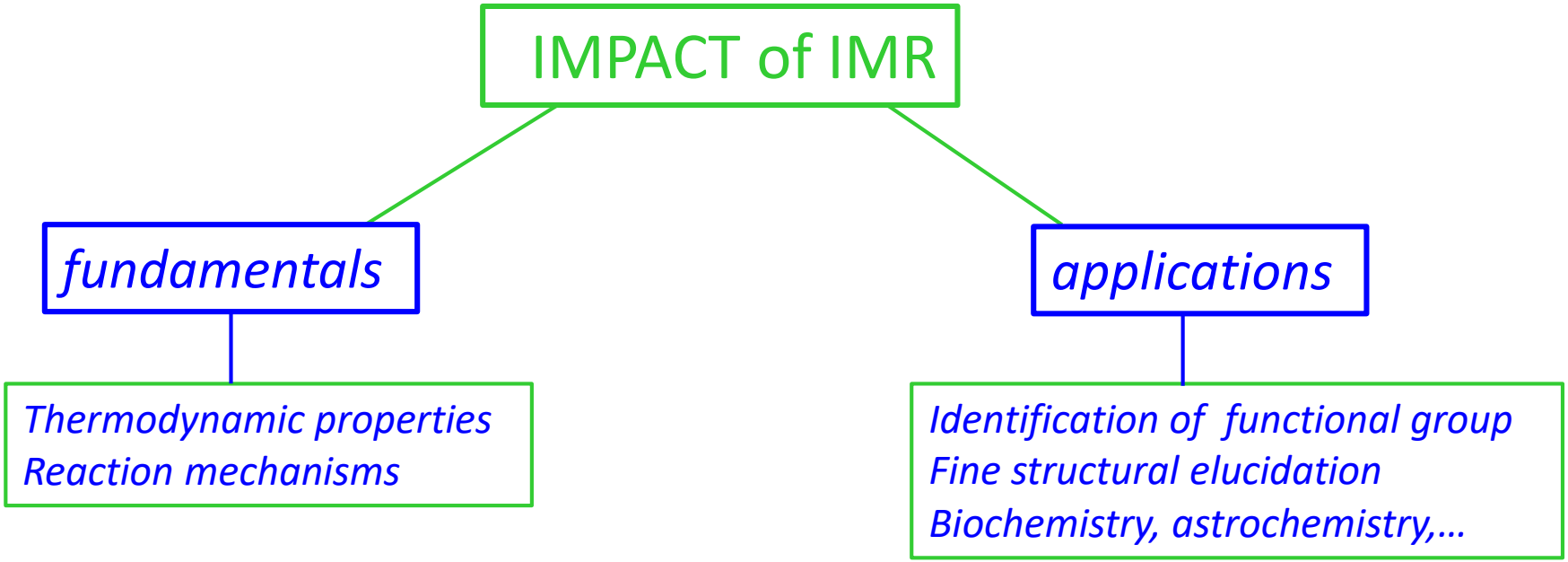

J. S. Brodbelt, Mass Spectrom. Rev. 1997; M. Eberlin, J.Mass Spectrom. 2006;
S. Gronert, Chem. Rev. 2001; V. Ryzhov, Anal. Chem. 2013;
H. I. Kenttamaa, Mass Spectrom. Rev. 2021

IMR by FT-ICR

Pros

- sensitivity
- specificity
- speed
- efficiency
- numerous reaction-based strategies
- no extensive purification/sample preparation
- (indirect) structural information

Cons

- inferred information on neutral products
- volatile neutrals (b.p. < 200 °C)

Gas phase ion molecule reactions

- **General aspects** (reaction efficiency; double-well potential energy surface)
- **Instrumentation**
- **IMR** (functional group-selective reactions; structurally diagnostic reactions)
- **Applications of IMR**

General aspects

Collision rate
the greatest possible reaction rate

← *number of charges in the ion*

↖ *dipole moment and polarizability of the neutral*

$$A^+ + B \underset{k_{-1}}{\overset{k_1}{\rightleftharpoons}} [AB]^+ \xrightarrow{k_2} C^+ + D$$

collision complex

Capture/collision rate : $k_{coll} \sim 1 \times 10^{-9}$ cm^3 molecule^{-1} s^{-1}

One or two order of magnitude larger than molecule-molecule reactions

How to calculate the k_{coll}

Calculations of collision rate constant

- Ion/induced dipole potential: **Langevin** theory
- Average dipole orientation (**ADO**) : Su & Bowers
- Angular momentum conserved ADO (**AADO**) : Su & Chesnavich

$$k_L = 2\pi e \left(\frac{\alpha}{\mu}\right)^{1/2}$$

capture rate coefficient

Langevin theory

α= polarizability

μ= the reduced mass of the pair

Interaction: ion-induced dipole

P. Langevin, *Ann. Chim. Phys. Ser.* 1905;
G. Giomousis, D. P. Stevenson, *J. Chem. Phys.* 1958

ADO theory

ADO: averaged dipole orientation

$$k_{ADO} = \frac{2\pi q}{\sqrt{\mu}} \left\{ \sqrt{\alpha} + C\mu_D \left(\frac{2}{\pi k_B T} \right)^{1/2} \right\}$$

the first term is the Langevin contribution

Interaction: ion- dipole

μ is the reduced mass; μ_D is the permanent dipole;
C is a correction factor depending on $\mu_D / \alpha^{1/2}$;
k_B is Boltzmann's constant
The dipole orientation is not considered

k_{ADO} predicts accurate Proton Transfer rate constants

T. Su, . T. Bowers, *J. Chem. Phys.* 1973; *Int. J. Mass Spectrom. Ion Phys.* 1973

k_{AADO} Theory

AADO: angular momentum conserved ADO

parametrized trajectory theory

- there is a net angular momentum transfer between the rotating molecule and the ion-molecule orbital motion.
- the AADO theory yields capture rate constants larger than ADO theory
- the AADO equation represents the best means to obtain an estimated capture rate for comparison with experimental reaction rate constants (± 10%) .

$$k_{AADO} = k_L\, G(x)$$

$$G(x) = \frac{(x+0.509)^2}{10.526} + 0.9754 \qquad x < 2$$

$$G(x) = (x+0.509)^2 + 0.9754 \qquad x \geq 2$$

empirical parametrization

$$x = \frac{\mu_D}{(8\pi\varepsilon_0\alpha k_B T)^{1/2}}$$

This equation makes it possible to approximate k_{coll} within ± 10%.

T. Su, . W. J. Chesnavich, *J. Chem. Phys.* 1982

Reaction Rates

$R^+ + N \longrightarrow P^+ +$ neutral products

$$-\frac{dR(t)}{dt} = k\, n\, R(t)$$ **bimolecular reaction**

n = number density of neutral N

In a conventional bimolecular process the number density of neutral reactant would decrease with time. Here, it does not.

$$I_{(t)} = I_0\, e^{-nkt}$$ pseudo-first order reaction

$$\ln \frac{I_{(t)}}{I_0} = -\, n\, k\, t \qquad k = k_{exp}$$

The total signal intensity is used to normalize the data and avoid errors from slight variations in the number of ions.

The signal intensity of $I_{(t)}$ can be monitored as a function of time and the rate constants for the disappearance of reactant ions and the appearance of product ions are obtained.

- The semilog plot of the decrease of the parent ion abundance with time is linearly interpolated and the **pseudo-first order rate constant** is obtained.
- The bimolecular rate constant (k_{exp}) at 300 K is gained from the ratio between the negative slope and ***n***, the number density of the neutral.
- ***n*** is calculated from the ideal gas equation and allows to convert the measured value of the neutral pressure (mbar) in molecule cm^{-3} at 300 K.

$$k_{exp} = \frac{\text{- slope } (s^{-1})}{n \text{ (molecule cm}^{-3})} = \ldots. \text{ cm}^3 \text{ molecule}^{-1} \text{ s}^{-1}$$

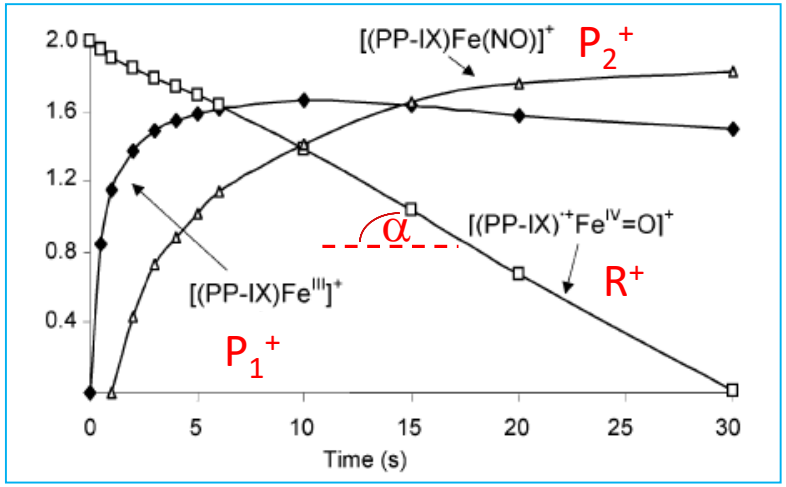

Figure 2. Plot of the logarithm of the relative ion abundances (%) versus time for the reaction of $(PP\text{-}IX)^{\bullet+}Fe^{IV}{=}O$ with NO at 3.0×10^{-8} mbar.

$$R^+ + NO \xrightarrow{OAT} P_1^+ + NO_2$$

$$P_1^+ + NO \xrightarrow{Add} P_2^+$$

Two consecutive reactions

Typically, the reproducibility of k_{exp} values is within 10%;

while the error in the absolute rate constants is estimated to be ± 30%.

It is mainly due to uncertainty in pressure measurements.

calibration of cold cathode gauge

$CH_4^{+\cdot} + CH_4 \longrightarrow CH_5^+ + CH_3$

$k_{CH4} = 1{,}1 \times 10^{-9}\ cm^3\ molecule\ s^{-1}$

time	I% m/z 16	I% m/z 17	ln 16
0	100.00	0.00	4.605
0.01	84.00	15.00	4.431
0.02	79.00	22.00	4.369
0.03	71.00	29.00	4.263
0.04	66.00	34.00	4.190
0.05	62.00	38.00	4.127
0.06	57.00	43.00	4.043
0.08	50.00	50.00	3.912
0.1	42.00	58.00	3.738
0.12	37.00	63.00	3.611
0.14	30.00	70.00	3.401
0.16	25.00	75.00	3.219
0.18	20.00	80.00	2.996
0.2	16.00	84.00	2.773
0.25	9.00	91.00	2.197
0.3	6.00	94.00	1.792
0.4	0.00	100.00	

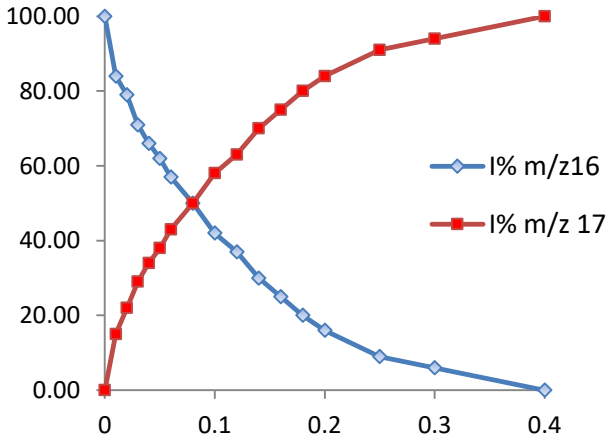

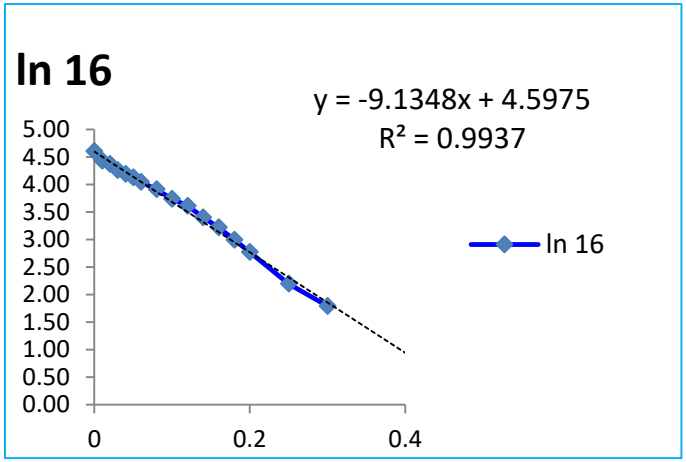

-slope

$$k_{exp} = \frac{9{,}13}{2{,}4 \times 10^{16} \times 1{,}1 \times 10^{-7}}\ cm^3\ molecule^{-1}\ s^{-1}$$

number density at 1.1×10^{-7} mbar

$K_{exp} / k_{CH4} = f$ (calibration factor)

The efficiency (Φ) of an ion molecule reaction can be determined by comparing the experimental rate constant (k_{exp}) with a theoretical estimate of the capture rate constant as percentages of the collision rate constant (k_{coll}).

$$\Phi = \frac{k_{exp}}{k_{coll}}$$

measure of reaction probability per collision
(number of events that bring to reaction)

Many exothermic reactions exhibit unit reaction probability at room T;

others proceed with reaction efficiency much less than unity.

Brauman double-well model

Many exothermic IMR have unit efficiency (fast reactions), others present very low efficiency (slow reactions)

Capture is a necessary but not sufficient condition for reaction…

slow means that most of the collisions simply return back to reactants

$$A^+ + B \underset{k_{-1}}{\overset{k_1}{\rightleftharpoons}} [AB]^+ \xrightarrow{k_2} C^+ + D$$

collision complex

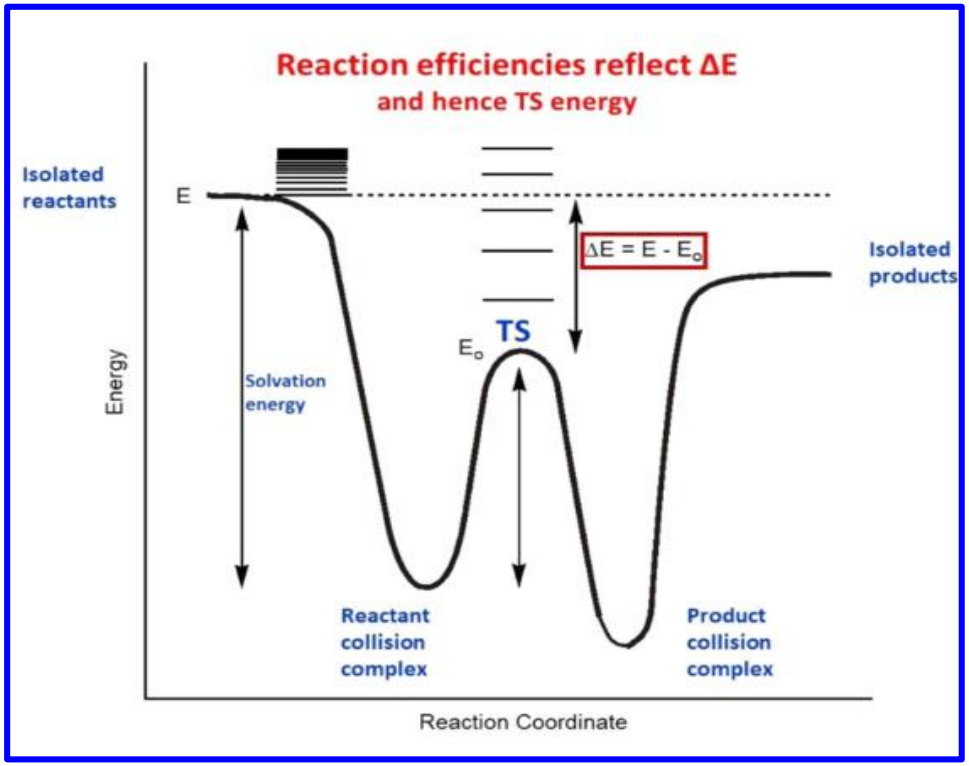

Only exothermic IMR with all barriers below the total energy level can proceed fast.

W. N. Olmstead, J. I. Brauman, *J. Am. Chem. Soc.* 1977

Overall, the efficiency depends on the height of the central barrier and the entropic constraints at the transition state.

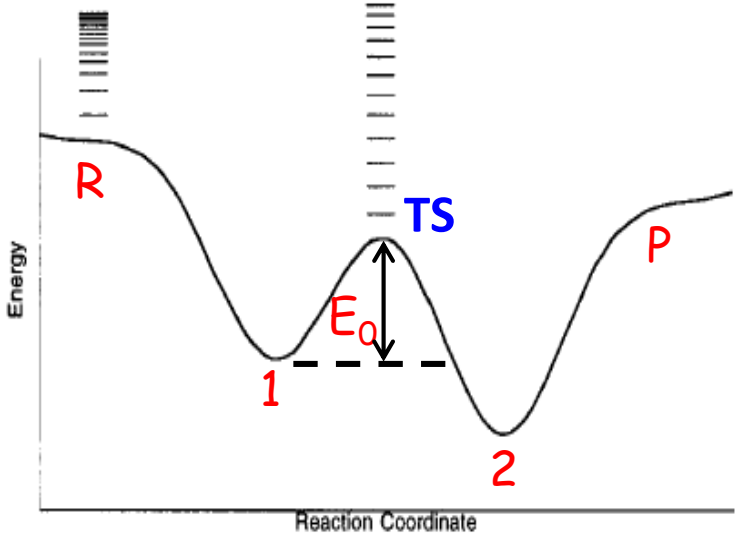

under the collisionless condition of FT-ICR, the intermediate complexes 1 and 2 are chemically activated

k_2: unimolecular isomerization with a *tight* (highy organized) TS (low A pre-exponential factor);
k_{-1} : fragmentation reaction with a *loose* (with many degrees of freedom) TS (high A pre-exponential factor)

TS may correspond to an entropic bottle-neck

competition takes place between one pathway that is energetically favored and another that is entropically favored.

energy favors k_2; entropy favors k_{-1}

At low E_0 a fast reaction will occur

S. Gronert, Chem. Rev. 2001

At high E_0 : (very) slow reaction

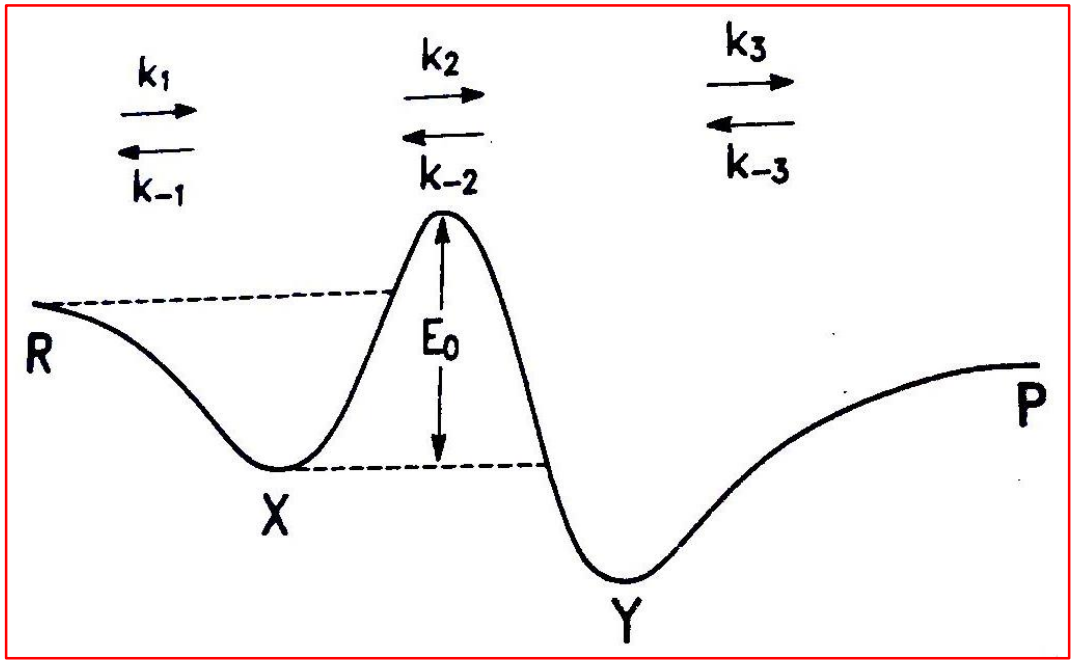

Slow reactions

k_{-1} will always be larger than k_2

At low pressure, double-minimum potential surface with TS lying above the reactants in energy : dissociation is energetically and entropically favored

For **long-lived** initial complexes, the energy can be removed *via* emission of a photon (**radiative stabilization**) and a slow reaction will be observed

Instrumental aspects

Where to perform IMR:

- Chemical ionization ion source
- Atmospheric pressure ion source
- rf-only quadrupole of a triple quadrupole
- Ion-trapping instruments: linear quadrupole ion-trap and FT-ICR (the most versatile MS)

In FT-ICR:

- low pressure measurements (10^{-5}-10^{-8} torr)
- reagent introduction with variable leak valves and/or pulsed valves
- time and energy control of reactions
- mass selection of reactant and product ions
- structural characterization by CID, ECD, IRMPD
- multistep MS^n sequences
- high resolution, high mass accuracy mode of operation

Multichannel Pulsed-Valves Inlet System

analytical chemistry

Article

Cite This: *Anal. Chem.* 2019, 91, 15652−15660

pubs.acs.org/ac

Integration of a Multichannel Pulsed-Valve Inlet System to a Linear Quadrupole Ion Trap Mass Spectrometer for the Rapid Consecutive Introduction of Nine Reagents for Diagnostic Ion/Molecule Reactions

John Y. Kong, Ryan T. Hilger, Chunfen Jin, Ravikiran Yerabolu, James R. Zimmerman, Randall W. Replogle, Tiffany M. Jarrell, Leah Easterling, Rashmi Kumar, and Hilkka I. Kenttämaa*

- rapid consecutive introduction of up 9 reagents
- automatic triggering allows to perform IMR on the HLPC time scale
- each component of a complex mixture: eluted, ionized, isolated, exposed to 9 different reagents

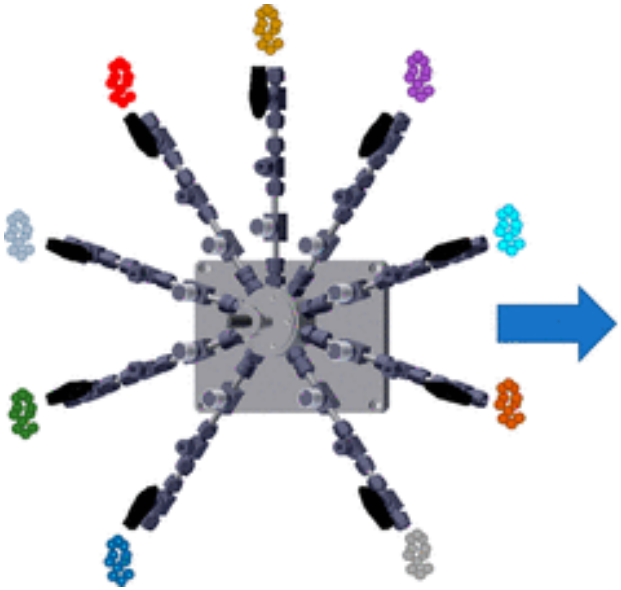

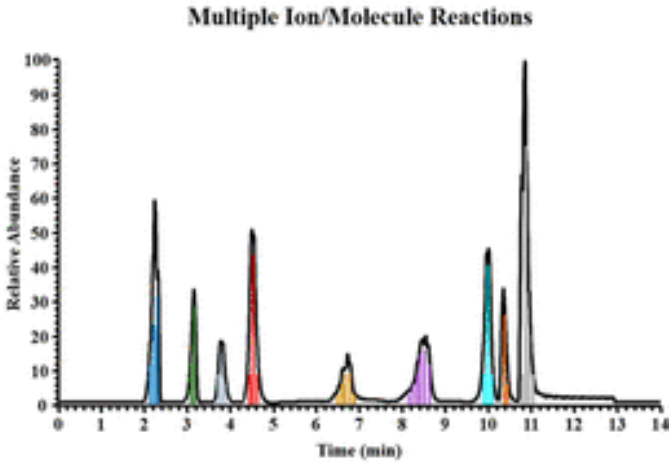

Bruker Apex II,
4.7T FT-ICR MS

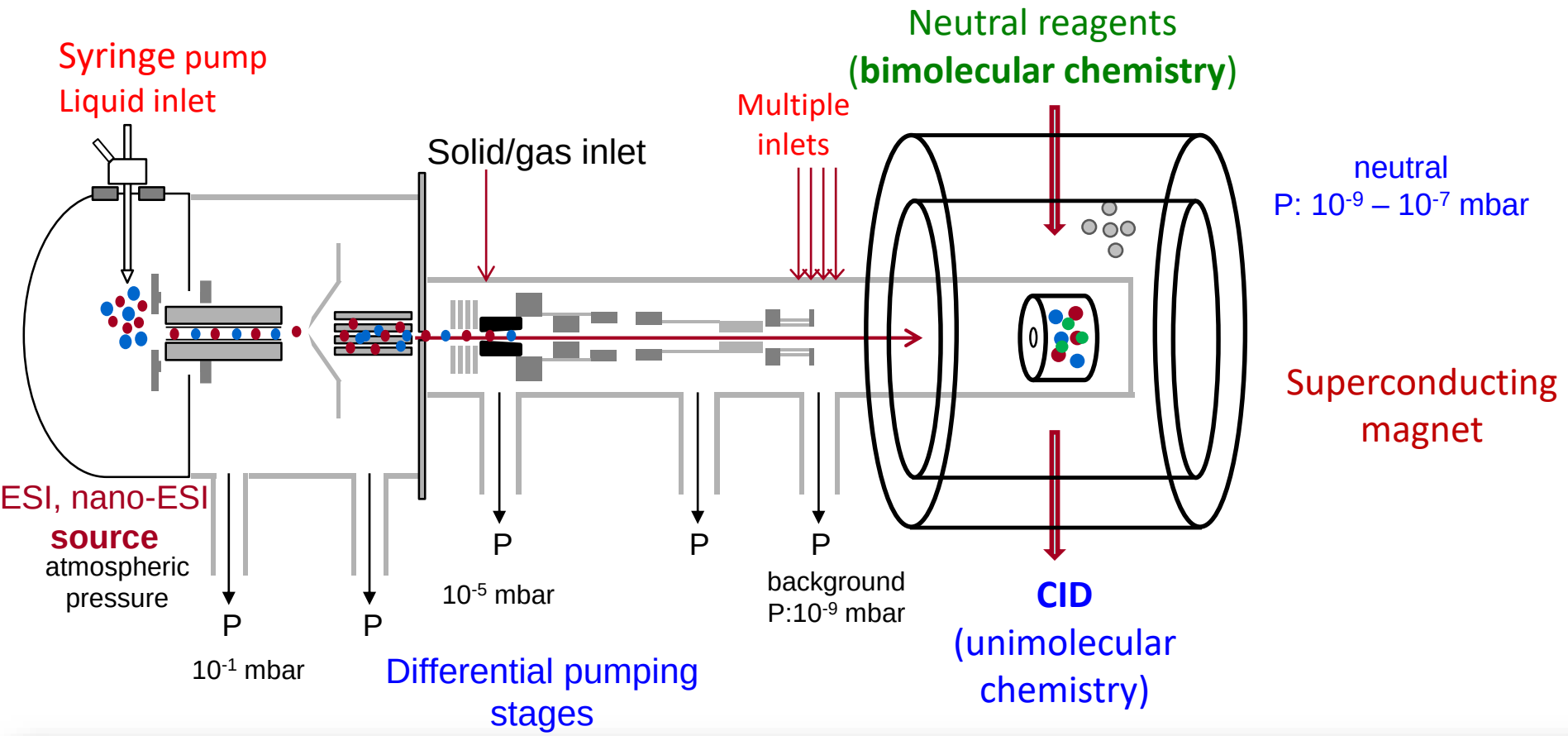

mass range extends in the low mass region down to 14.5 Da

Equipment for TNA in Roma

Types of Ion-Molecule Reactions

- Electron-Transfer
- Proton transfer
- H-atom/ O-atom transfer
- H/D exchange
- Functional-group selective
- Nucleophilic displacement
- Radiative association

V. Ryzhov, *Anal. Chem*. 2013; H. I. Kenttämaa, *Mass Spectrom. Rev.* 2021

Electron-Transfer Reactions

HNO^+ is more stable than HON^+ by 16.7 kcal/mol; isomerization requires 55.7 kcal/mol.

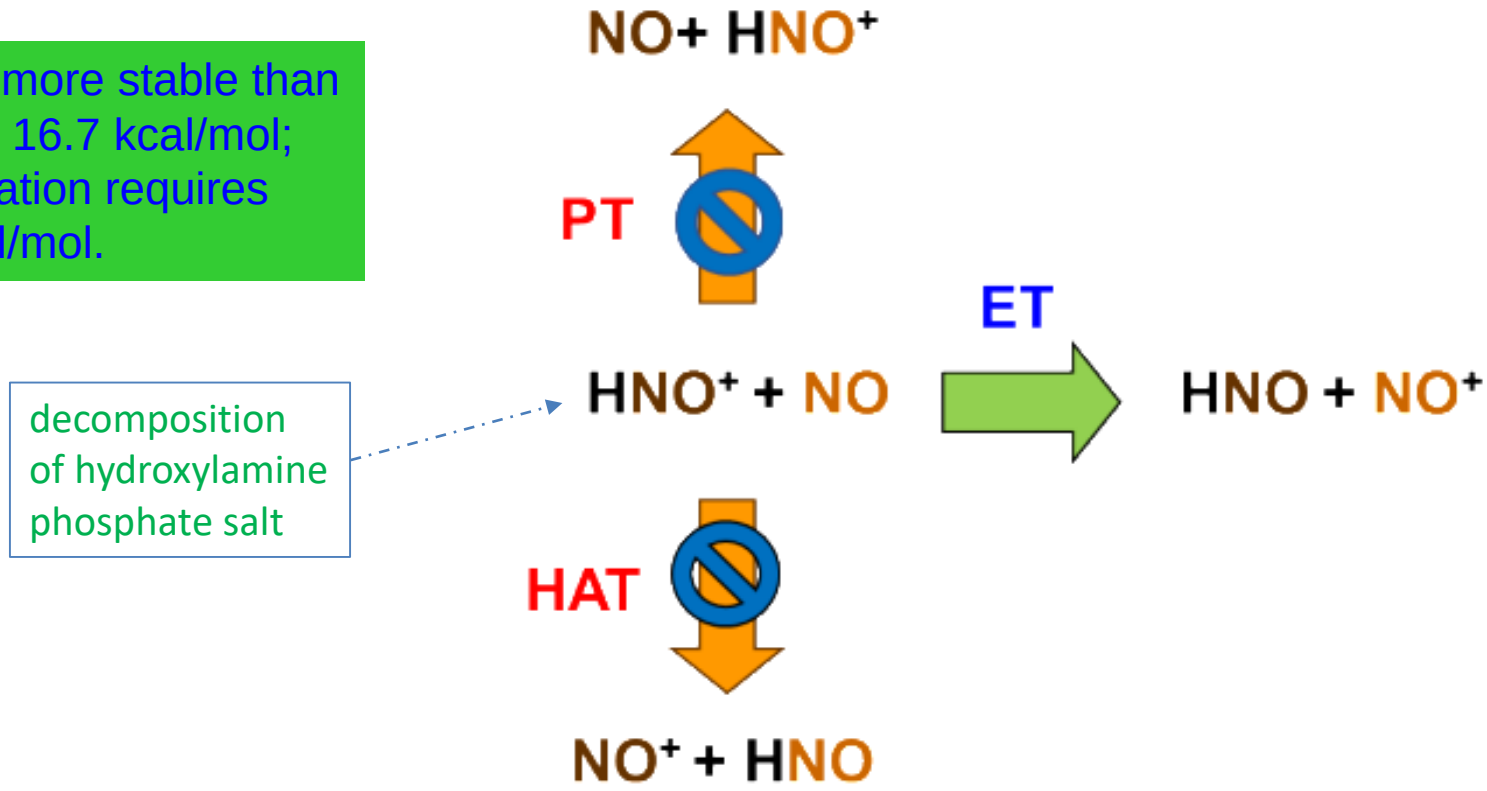

decomposition of hydroxylamine phosphate salt

calculations at the CCSD(T)/augccpVTZ//B3LYP/def2-TZVP level of theory

U. Dandamudi, M.E. Crestoni, S. Fornarini, 2021, *submitted*

Proton-Transfer Reactions

$$AH^+ + B \rightleftharpoons BH^+ + A$$

$$A^- + BH \rightleftharpoons AH + B^-$$

base A of unknown GB (PA)

base B of known GB (PA)

by using several reference bases B, **the GB (PA) of A can be determined**

Bracketing method: kinetics

$$AH^+ + B \longrightarrow BH^+ + A$$

- measurement of k_{exp}
- presence of gaseous B

Equilibrium method: equilibrium

$$AH^+ + B \rightleftharpoons BH^+ + A$$

- measurement of K_{eq}
- presence of gaseous A and B

$$K_{eq} = \frac{[BH]^+ [A]}{[AH]^+ [B]} \qquad \ln K_{eq} = \frac{-\Delta G^\circ}{RT}$$

G. Bouchoux, Int. J. Mass Spectrom. Ion Processes 1996

Chiral recognition in deprotonation reactions

J. Am. Chem. Soc. **1996,** *118,* 8751−8752

Chiral Recognition Is Observed in the Deprotonation Reaction of Cytochrome *c* by (2*R*)- and (2*S*)-2-Butylamine

Elvira Camara, M. Kirk Green, Sharron G. Penn, and Carlito B. Lebrilla*

Department of Chemistry, University of California Davis, California 95616

cyt c + (2R)/(2S)-2-butylamine
(9+, 8+, 7+)

- (2R)- 10 times greater than (2S)-
- one reacting species for 9^+ and two for 8^+ and 7^+ : different conformers

chiral probes of gas-phase structures provide :
- indirect information on protein structures (intermediates of defined structures) and
- thermochemical data about individual sites in large (bio)molecules

C. B. Lebrilla et al., J. Am. Chem. Soc. 1996; J. Am. Chem. Soc. 1998; M. Speranza et al. Chiral. 2009

OAT from the naked core of Cpd I

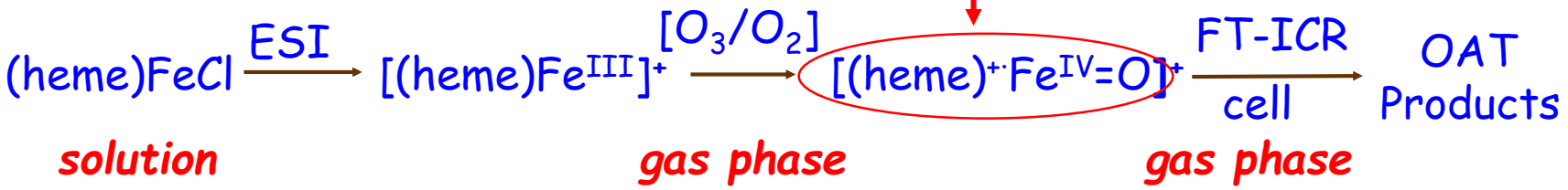

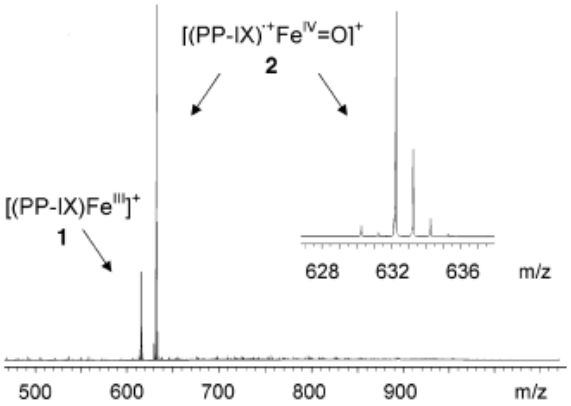

Figure 1. ESI FT-ICR mass spectrum from a methanol solution of (PP-IX)FeCl (10 μM), admitting O_3/O_2 in the capillary/skimmer interface of the ESI source. The inset is an enlargement of the spectrum displaying signals characteristic of $(PP\text{-}IX)^{\bullet+}Fe^{IV}$=O ions (2).

Ion-molecule reactions of $[(heme)^{+\cdot}Fe^{IV}=O]^+$

Table 1. Gas-Phase Reactivity of Selected Substrates (L) with $(PP\text{-}IX)^{\bullet+}Fe^{IV}(O)^+$ (**2**) Formed by the Reaction of $Fe(PP\text{-}IX)^+$ (**1**) with O_3

L	k_{exp}[a]	Φ[b]	product ions **1**/(PP-IX)Fe(O)(L)$^+$
NO	3.0	4.2	100/0
NO_2	1.9	2.9	100/0
propyne	0.036	0.027	100/0
Me_2S	1.7	1.3	80/20
Me_2S_2	2.8	2.4	90/10
pyridine	2.4	1.7	100/0
$P(OMe)_3$	8.6	7.3	95/5

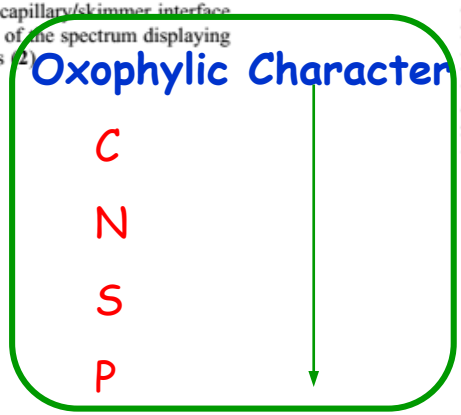

M. E. Crestoni, S. Fornarini, *Inorg. Chem.* **2007**

OAT by Mn(V)-Oxo porphyrin complex

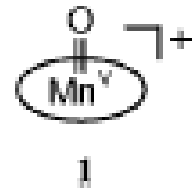

1

Mn^{V}-oxo-porphyrin complexes prepared in aqueous solution: diamagnetic d^2 low-spin ground state

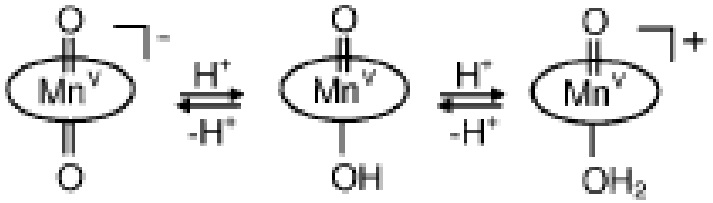

high pH low pH

The OAT reactivity in water is found to be strongly pH-dependent: prototropic equilibria

$$[(TPFPP)MnCl]^{+} + PhIO \xrightarrow{ESI} [(TPFPP)Mn^{V}O]^{+} + L \xrightarrow{FT\text{-}ICR} [(TPFPP)Mn^{III}]^{+} + LO$$

solution, -20°C *gas phase*

L = propene, (E)-2-butene, (Z)-2-butene, styrene, cyclohexene, 1,3,5-CHT, (+)-camphene, indene, β-pinene, (R)-(+)-limonene. OAT reactivty increases with the olefin's IE value

M. E. Crestoni, et al. *Chem. Eur. J. 2009*

Properties of biomimetic models of enzymatic reaction intermediates by IMR

J|A|C|S
ARTICLES
Published on Web 02/16/2008

Probing the Compound I-like Reactivity of a Bare High-Valent Oxo Iron Porphyrin Complex: The Oxidation of Tertiary Amines

Barbara Chiavarino,† Romano Cipollini,† Maria Elisa Crestoni,† Simonetta Fornarini,*,† Francesco Lanucara,† and Andrea Lapi‡

high-valent iron(IV)-oxo porphyrin radical cation complex

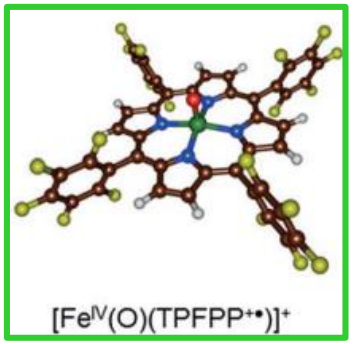

Chemical Science

EDGE ARTICLE

Cite this: *Chem. Sci.*, 2015, 6, 1516

A comprehensive test set of epoxidation rate constants for iron(IV)–oxo porphyrin cation radical complexes†

Mala A. Sainna,[a] Suresh Kumar,[b] Devesh Kumar,*[b] Simonetta Fornarini,*[c] Maria Elisa Crestoni*[c] and Sam P. de Visser*[a]

ChemPubSoc Europe
DOI: 10.1002/chem.201604361
CHEMISTRY A European Journal Full Paper

Reaction Mechanisms

A Systematic Account on Aromatic Hydroxylation by a Cytochrome P450 Model Compound I: A Low-Pressure Mass Spectrometry and Computational Study

Fabián G. Cantú Reinhard+,[a] Mala A. Sainna+,[a] Pranav Upadhyay,[b] G. Alex Balan,[a] Devesh Kumar,[b] Simonetta Fornarini,*[c] Maria Elisa Crestoni,*[c] and Sam P. de Visser*[a]

ChemPubSoc Europe
DOI: 10.1002/ejic.201800273
EurJIC Full Paper

Enzyme Models

Hydrogen Atom vs. Hydride Transfer in Cytochrome P450 Oxidations: A Combined Mass Spectrometry and Computational Study

Fabián G. Cantú Reinhard,[a] Simonetta Fornarini*[b] Maria Elisa Crestoni*[b] and Sam P. de Visser*[a]

M. E. Crestoni, S. Fornarini, *J.Am.Chem.Soc.* 2008; S. Fornarini, M. E. Crestoni, S. De Visser, *Chem. Science* 2015; *Chem Eur. J.* 2016; *EurJIC* 2018

Functional-group selective IMR

Anal. Chem. **2004,** *76,* 964−976

Ion−Molecule Reactions for Mass Spectrometric Identification of Functional Groups in Protonated Oxygen-Containing Monofunctional Compounds

Michael A. Watkins,[†] Jason M. Price,[†,‡] Brian E. Winger,[§] and Hilkka I. Kenttämaa*,[†]

1) ethyl vinyl ether
2) diethylmethoxyborane

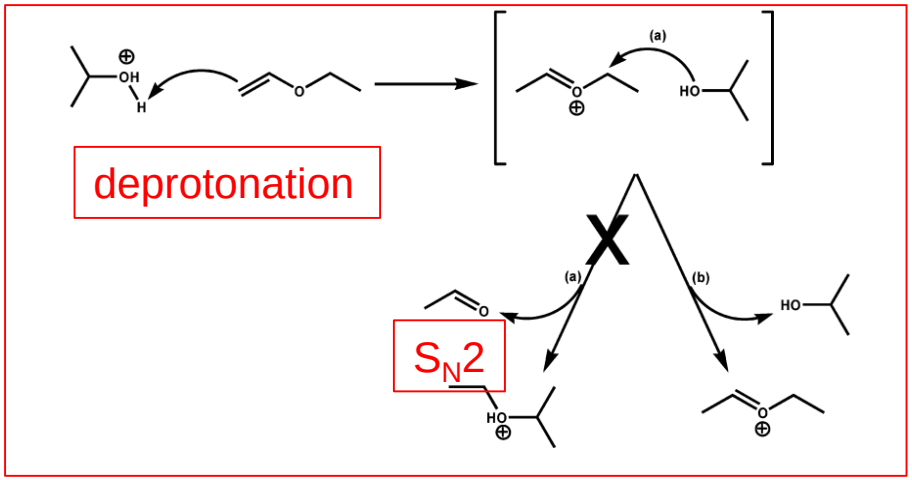

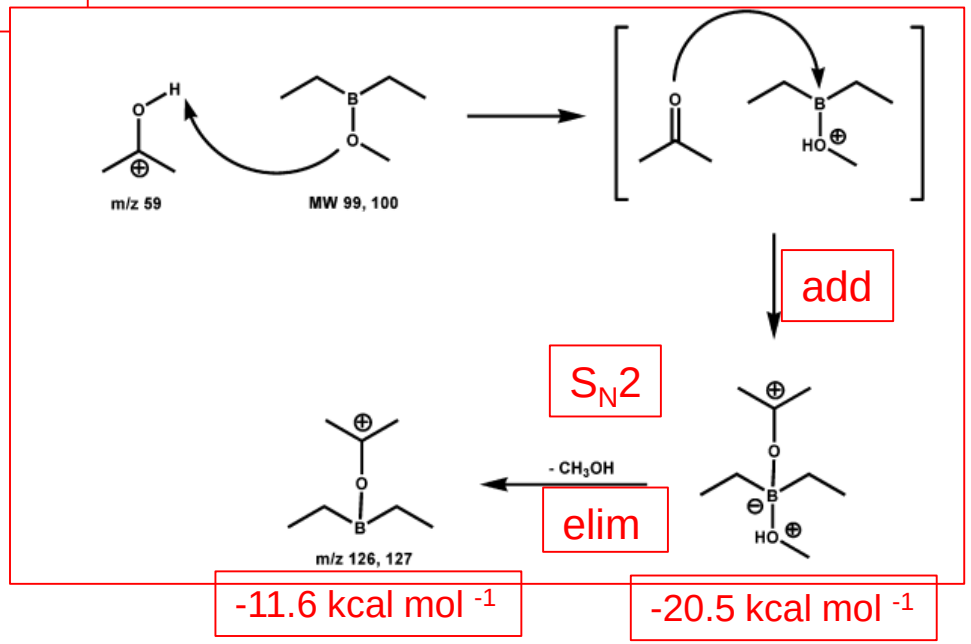

diethylmethoxyborane reacts with protonated monofunctional oxygen-containing analytes (**alcohols, ketones, aldehydes, esters, ethers, carboxylic acids, amides**) by deprotonation followed by substitution of methanol: provides structure elucidation for unknown mixture components

H. I. Kenttamaa, *Anal. Chem. 2004;* M. N. Eberlin, *J. Mass Spectrom*. 2006; H. I. Kenttämaa, *Mass Spectrom. Rev.* 2021

Identification of N-oxide and sulfoxide functionalities in protonated drug metabolites by using IMR

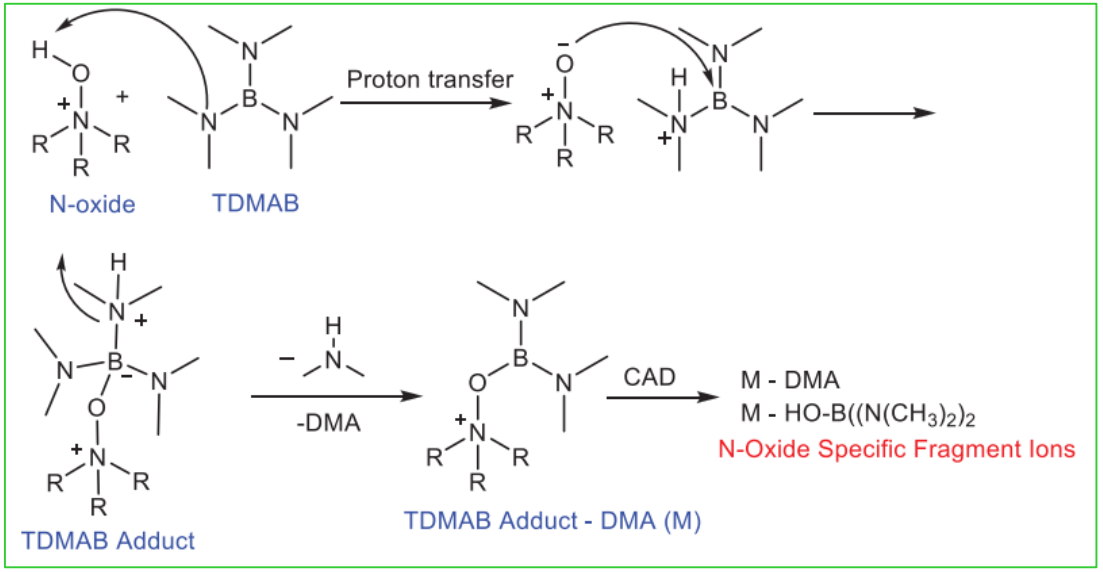

PA (TDMAB) = 230 kcal/mol
PA (N-oxides) = 220-240 kcal/mol
PA (sulfoxides) = 215-220 kcal/mol

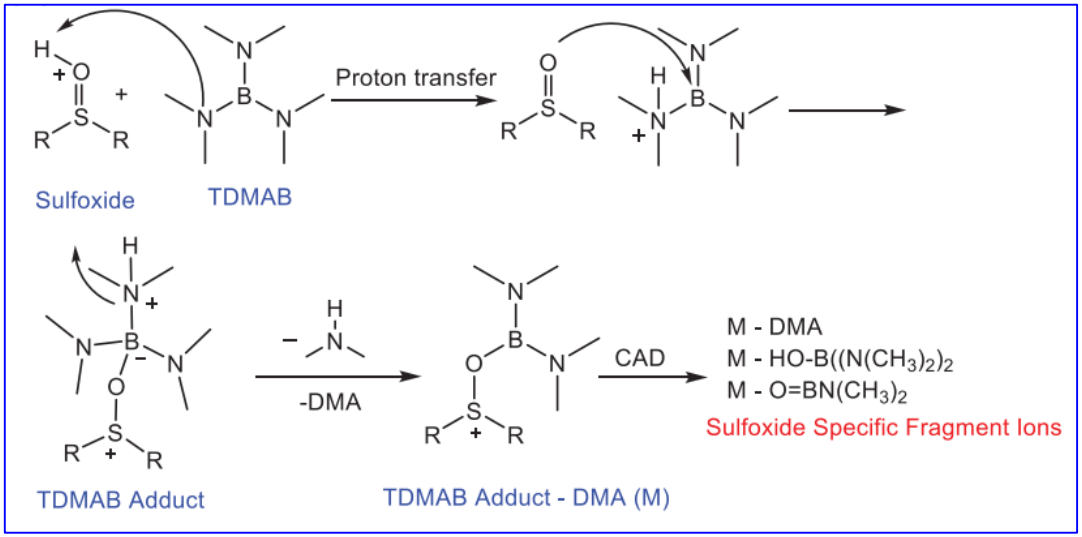

H. I. Kenttämaa, *J. Org. Chem.* 2016

Application to antipsychotics drug metabolites

Journal of Pharmaceutical and Biomedical Analysis 51 (2010) 805–811

Contents lists available at ScienceDirect

Journal of Pharmaceutical and Biomedical Analysis

journal homepage: www.elsevier.com/locate/jpba

Liquid chromatography/tandem mass spectrometry utilizing ion-molecule reactions and collision-activated dissociation for the identification of N-oxide drug metabolites

Steven C. Habicht, Penggao Duan[1], Nelson R. Vinueza, Mingkun Fu, Hilkka I. Kenttämaa*

Department of Chemistry, Purdue University, West Lafayette, IN 47907, USA

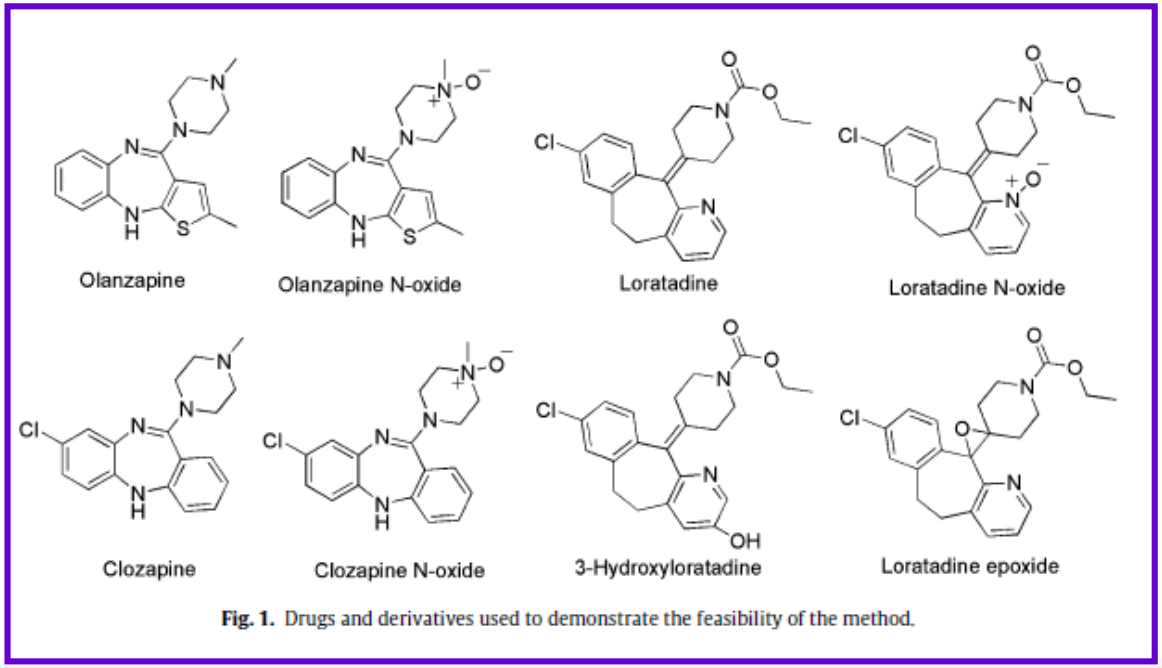

Fig. 1. Drugs and derivatives used to demonstrate the feasibility of the method.

Functional-group selective IMR

Research Article

Rapid Communications in Mass Spectrometry

Received: 25 January 2014 Revised: 27 February 2014 Accepted: 27 February 2014 Published online in Wiley Online Library

Rapid Commun. Mass Spectrom. **2014**, *28*, 1107–1116
(wileyonlinelibrary.com) DOI: 10.1002/rcm.6884

Probing the exposure of the phosphate group in modified amino acids and peptides by ion-molecule reactions with triethoxyborane in Fourier transform ion cyclotron resonance mass spectrometry

Francesco Lanucara[1,2*], Simonetta Fornarini[3], Claire E. Eyers[2] and Maria Elisa Crestoni[3]

$$[\text{Peptide-O-P(O)(OH)}_2\text{+nH}]^{n+} + \text{B(OR)}_3 \rightarrow [\text{Peptide-O-PO(OH)OB(OR)}_2\text{+nH}]^{n+} + \text{ROH}$$

Scheme 1. Addition-elimination reaction of phosphorylated amino acids and peptides with alkoxyboranes $B(OR)_3$.

Potential to measure the effect of local environment, the exposure and accessibility of a phosphate moiety on the surface of a biomolecule and to distinguish positional phosphorylated peptide isomers

The reaction efficiency allows to explore the accessibility of phosphate groups in biomolecules

Hydrolysis of cis and transplatin

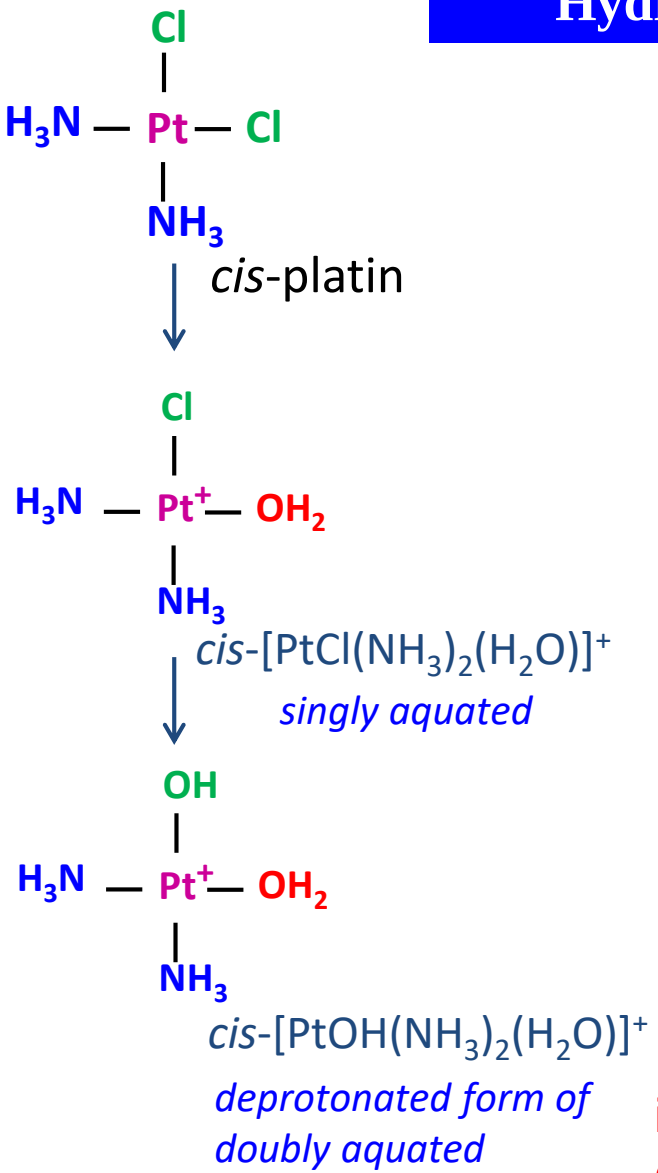

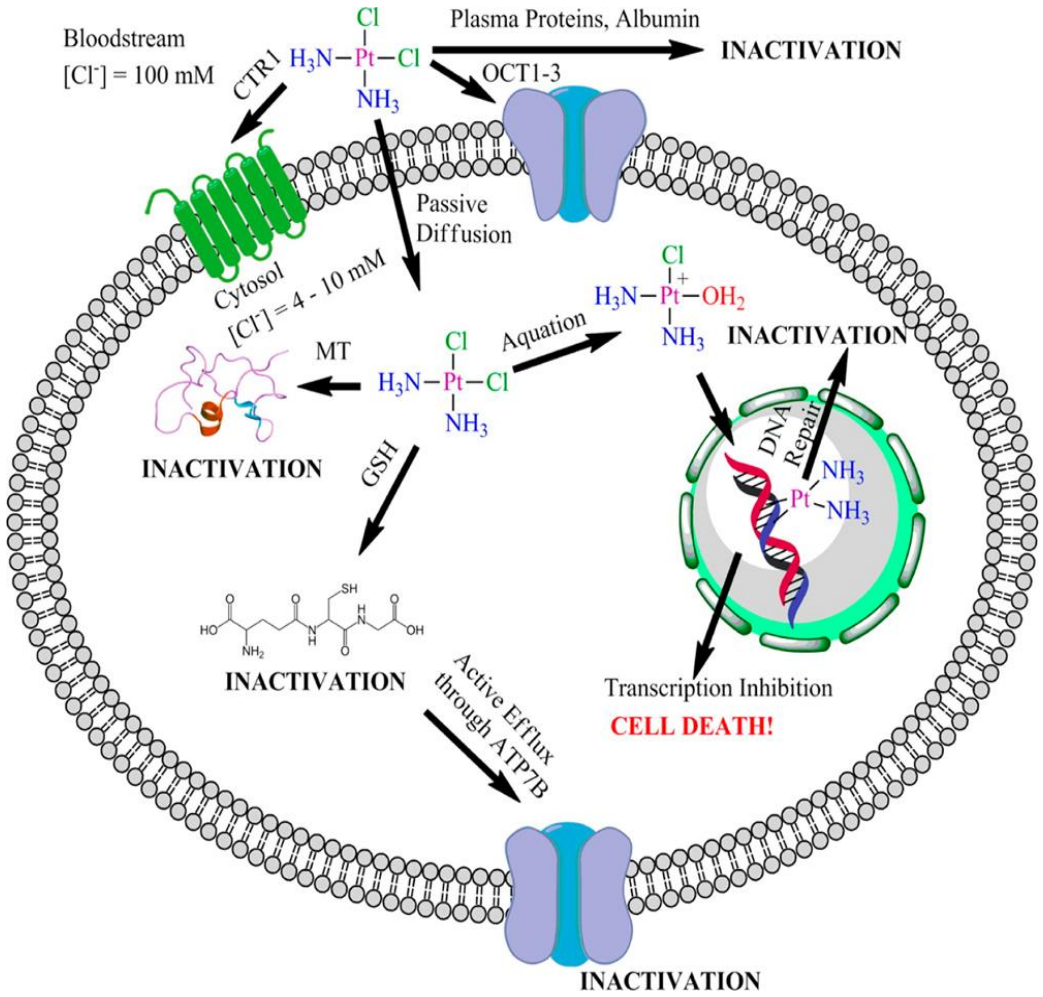

in solution it is not easy to separate the influence of the nature of the incoming and leaving ligands

S. Fornarini et al., RSC Adv. 2017

cis/trans-$[PtX(NH_3)_2(H_2O)]^+$ + L ⟶ *cis/trans*-$[PtX(NH_3)_2(L)]^+$ + H_2O

(X=Cl, OH)

In solution, formation of hydroxo-bridged polynuclear complexes.

Table 2 Reactivity of $[PtX(NH_3)_2(H_2O)]^+$ (X = Cl, OH; *cis* and *trans* isomers) with simple molecules in the gas-phase

Reagent ion	Neutral	k_{exp}[a]	Eff[b] (%)
cis-$[PtCl(NH_3)_2(H_2O)]^+$	TMP	3.7	2.5[b]
	Pyridine	0.6	0.41[b,c]
	Thioanisole	1.4	1.1[b]
	Dimethylsulfide	0.034	0.026
trans-$[PtCl(NH_3)_2(H_2O)]^+$	TMP	3.3	2.3
	Pyridine	1.4	0.93[d]
	Thioanisole	7.7	6.3
	Dimethylsulfide	2.4	1.7
cis-$[Pt(OH)(NH_3)_2(H_2O)]^+$	TMP	0.96	0.66
	Pyridine	0.46	0.31[e]
	Thioanisole	0.1	0.08
	Dimethylsulfide	n. r.[f]	
trans-$[Pt(OH)(NH_3)_2(H_2O)]^+$	TMP	1.1	0.78
	Pyridine	0.05	0.03[g]
	Thioanisole	0.46	0.37
	Dimethylsulfide	n. r.[f]	

[a] Second order rate constant in units of 10^{-11} cm^3 s^{-1} at 298 K, estimated error ±30%. Other sampled compounds proved to be

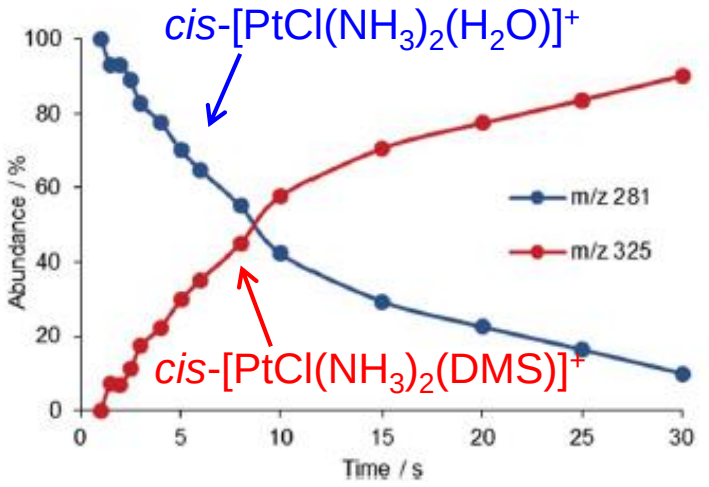

- ligand exchange; low efficiencies
- Cl complexes more reactive than OH
- TMP more reactive than TA
- *trans*Pt more reactive than *cis*Pt vs S ligands

S. Fornarini et al., RSC Adv. 2017

The ligand exchange is a stepwise process

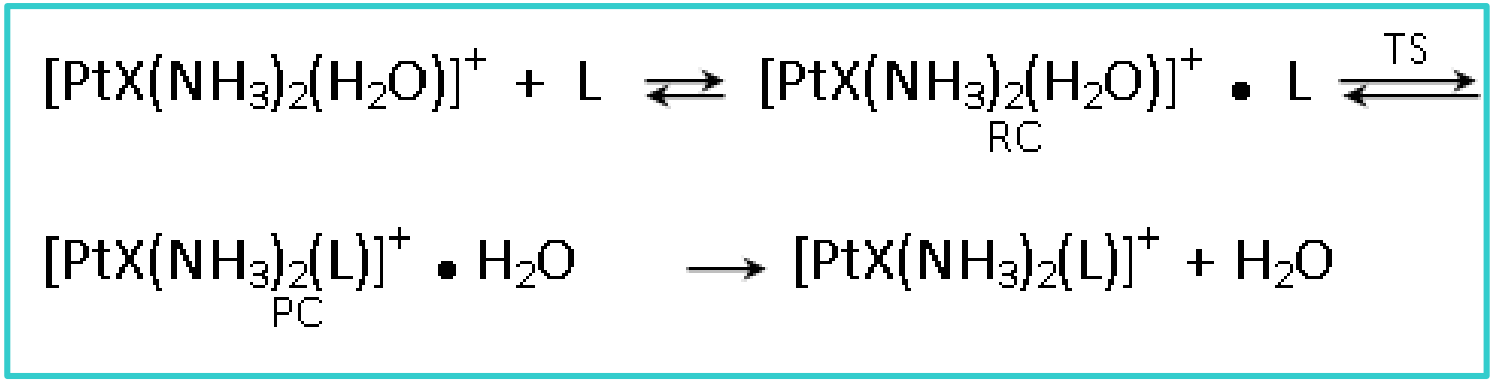

The Φ of the overall process depends on the branching of RC

S. Fornarini et al., RSC Adv. 2017

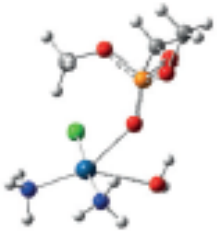

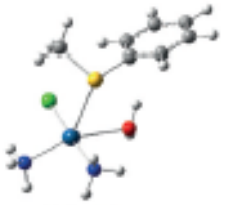

PES for the reaction of *cis*-$[PtCl(NH_3)_2(H_2O)]^+$ with L= TMP, TA. Relative enthalpies (kJ mol^{-1}) at 298 K are reported at the wB97X-D/6-311+G(d,p) level of theory.

Ligand exchange of water by TA is kinetically more favored in the *trans*- with respect to the *cis*-isomers

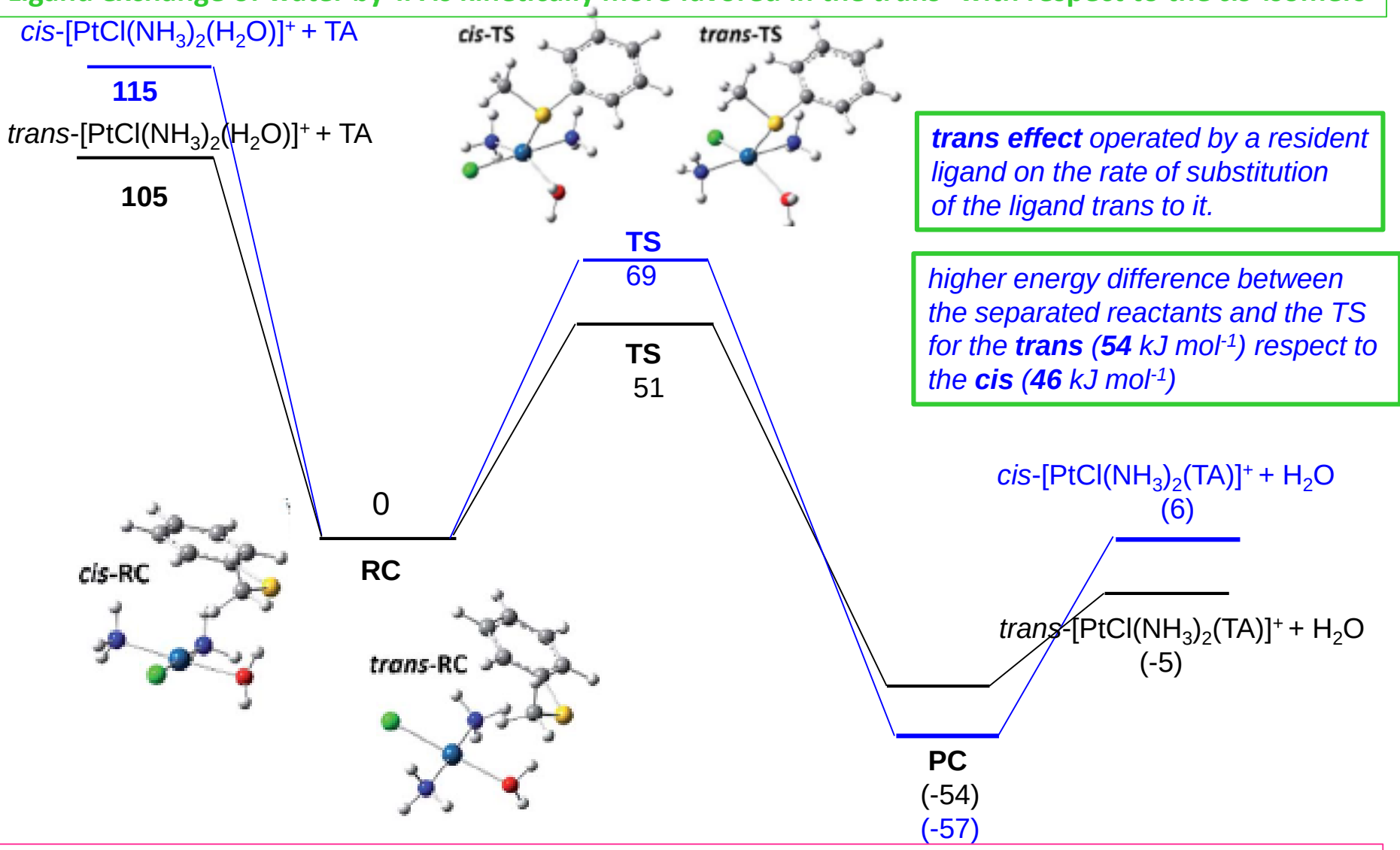

trans effect *operated by a resident ligand on the rate of substitution of the ligand trans to it.*

higher energy difference between the separated reactants and the TS for the ***trans*** *(**54** kJ mol^{-1}) respect to the* ***cis*** *(**46** kJ mol^{-1})*

water is displaced by TA more easily when the trans-site is occupied by a Cl than by NH_3, according to *trans*-directing sequence $Cl^- > NH_3$

S. Fornarini et al., RSC Adv. 2017

Association Reactions

- solvation of an ion by weak electrostatic forces or hydrogen bonding;
- ion ligation involving bonds of intermediate strength;
- strong chemical bond formation

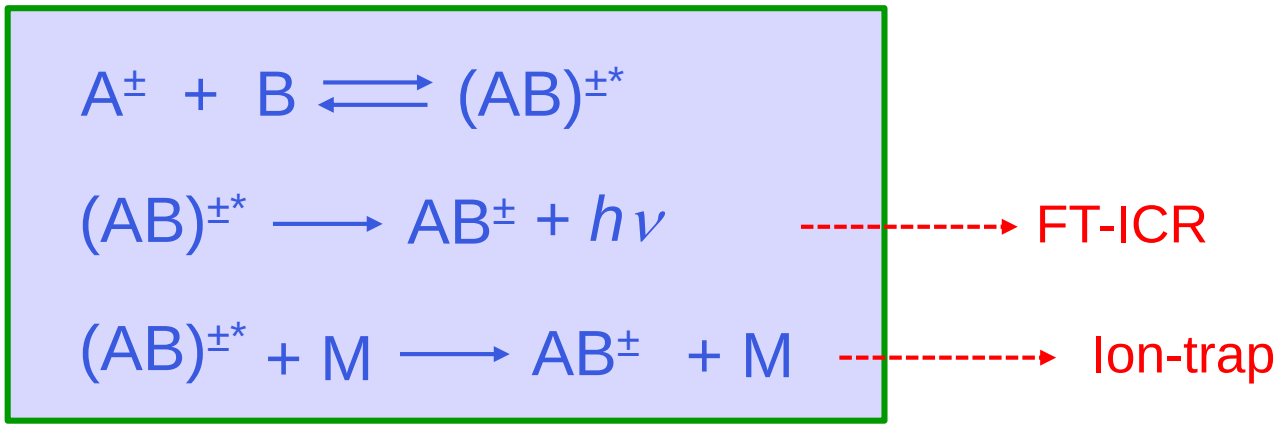

at the low operating pressures of the FT-ICR cell: thermal equilibration of the adduct ion via IR radiative emission

The rate of radiative emission is expected to increase with increasing size of the ion

F.W. Mc Lafferty et al., *J. Am. Chem. Soc. 2001*

Functional-group selective IMR

J Biol Inorg Chem (2007) 12:22–35
DOI 10.1007/s00775-006-0159-9

ORIGINAL PAPER

Heme-peptide/protein ions and phosphorous ligands: search for site-specific addition reactions

Maria Elisa Crestoni · Simonetta Fornarini

- **Fe(III)-heme$^+$**
- **MP11**
- **cyt c**
- **myoglobin**

+ $OP(OMe)_3$ (GB: 206 kcal/mol)
+ $P(OMe)_3$ (GB: 215.3 kcal/mol)

the addition of phosphite is limited to just one molecule, irrespective of charge state, in contrast with a charge-dependent number of added phosphate ligands

- **$OP(OMe)_3$ is engaged in H bonding to protonated sites**
- **$P(OMe)_3$ is sampling the protein prosthetic group**

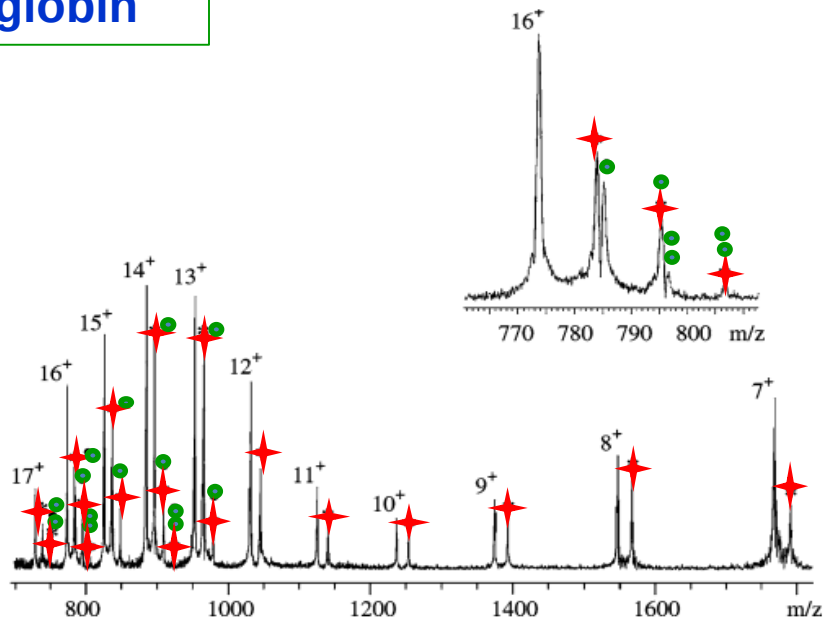

Fig. 9 FT-ICR mass spectrum of cyt *c* allowed to react with a 70:30 mixture of triethylphosphite, $P(OEt)_3$, and triethylphosphate, $OP(OEt)_3$, at 2.4×10^{-8} mbar for 3 s. *Numbers* denote the charge states of cyt *c* ions. Each charge state forms adducts with a single $P(OEt)_3$ molecule (represented by a *star*). The high charge states add up to four $OP(OEt)_3$ molecules; each $OP(OMe)_3$ molecule is represented by a *circle*

(J Am Soc Mass Spectrom 2005, 16, 589–598)

Binding of Gaseous Fe(III)-Heme Cation to Model Biological Molecules: Direct Association and Ligand Transfer Reactions

Fausto Angelelli, Barbara Chiavarino, Maria Elisa Crestoni, and Simonetta Fornarini

Department of Studies on Chemistry and Technology of Biologically Active Substances, University of Rome, "La Sapienza," Rome, Italy

Ligand association equilibrium

$$\text{Fe(III)-heme}^+ + \text{L} \underset{k_{-1}}{\overset{k_1}{\rightleftarrows}} \text{Fe(III)-heme(L)}^+$$

L= NO, amines, carbonyl compounds, ethers, nitriles, sulfides, phosphoryl compounds

$$HCB(L) = -\Delta G^\circ = -RT\ln K_{eq}$$

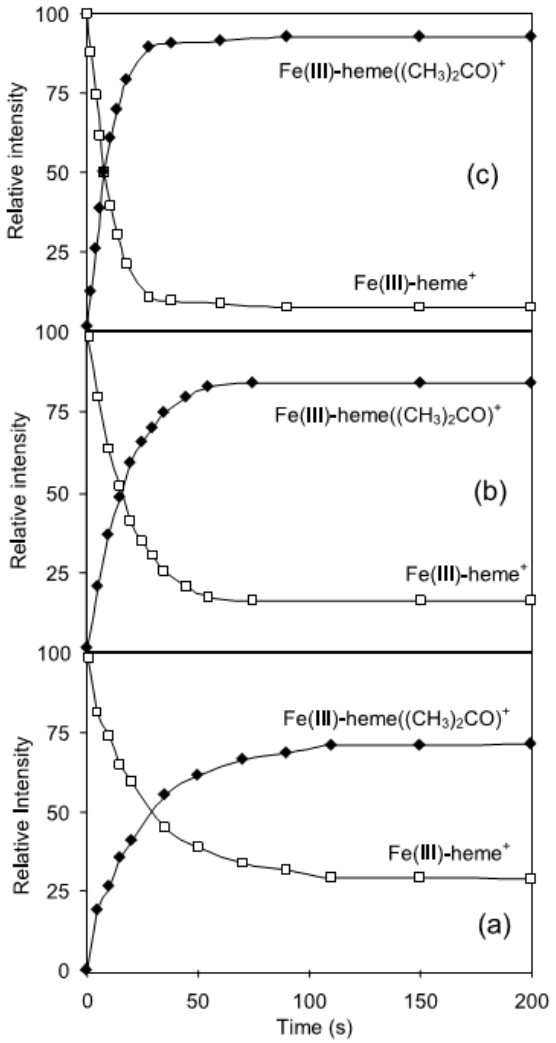

Figure 5. Time dependence of ion abundances for the Fe(III)-heme$^+$ ion reaction with acetone at 5.2×10^{-8} mbar (**a**), 8.7×10^{-8} mbar (**b**), 2.1×10^{-7} mbar (**c**).

Ligand transfer equilibria

$$Fe(III)\text{-heme}(L_1)^+ + L_2 \rightleftarrows Fe(III)\text{-heme}(L_2)^+ + L_1$$

$$HCB(L_1) - HCB(L_2) = -\Delta G^\circ = -RT\ln K_{eq}$$

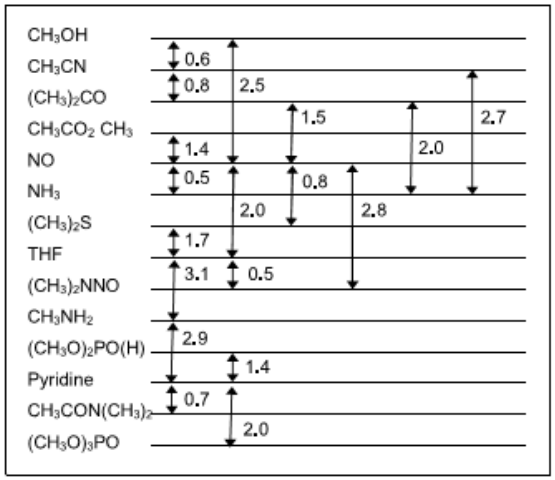

Figure 7. ΔG_5° (kcal mol^{-1}, 300 K) ladder for the Fe(III)-heme transfer reactions between selected pairs of ligands. The values in the ladder correspond to HCB differences for each couple of ligands.

Table 6. Free energy changes for gas-phase ligand binding toward H^+ and Fe(III)-heme$^+$

L	GB[a]	HCB[b]
CH_3OH	173.2	13.1
CH_3CN	179.0	13.7
$(CH_3)_2CO$	186.9	14.6
CH_3CO_2 CH_3	189.0	14.8
NO	120.8	16.1
NH_3	195.7	16.6
$(CH_3)_2S$	191.5	16.9
Tetrahydrofuran	189.9	18.1
$(CH_3)_2N$-NO	203.0[c]	18.9
CH_3NH_2	206.6	21.2
$(CH_3O)_2PO(H)$	206.1	22.7
Pyridine	214.7	24.1
$CH_3CON(CH_3)_2$	209.6	24.8
$(CH_3O)_3PO$	205.7	26.1

NO stands out as a superior ligand

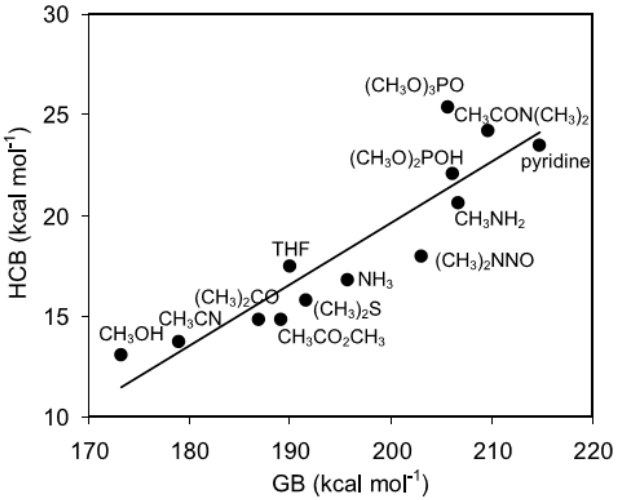

Figure 9. General correlation between Fe(III)-heme$^+$ cation b sicities (HCB, equal to $-\Delta G_1^\circ$ for the ligand association reactio and gas phase basicity toward the proton (GB) values.

A linear correlation between HCBs and ΔGBs of the ligands suggests that similar effects play a role when a lone pair donor binds to a proton or to Fe(III)heme$^+$

SAPIENZA
UNIVERSITÀ DI ROMA

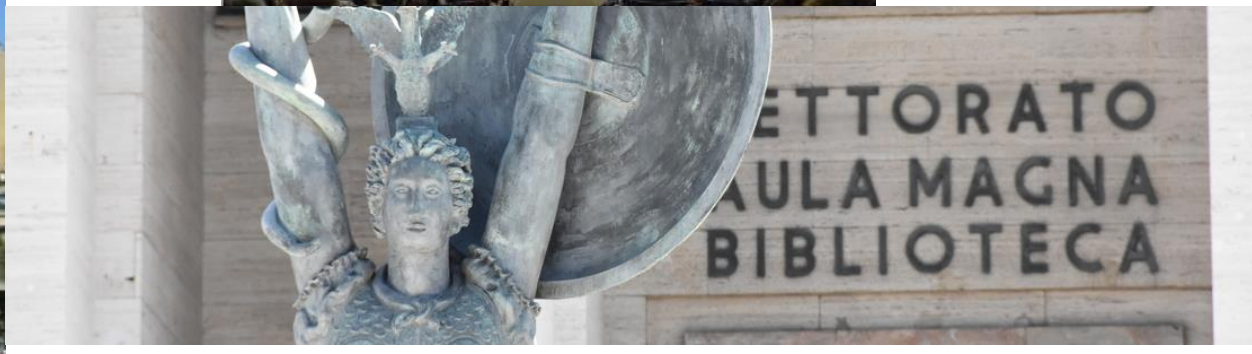

Dip. CTF

Simonetta Fornarini

Barbara Chiavarino

Davide Corinti

Alessandro Maccelli

Alba Lasalvia

Valentina Lilla

SAPIENZA
UNIVERSITÀ DI ROMA

EU FT-ICR MS

Thank you for the kind attention